

**MARBLE DIKES IN THE OLKHON COMPOSITE TERRANE (WEST BAIKAL AREA)**E.V. Sklyarov ¹✉, A.V. Lavrenchuk ^{2,3}, A.M. Mazukabzov ¹

¹ Institute of the Earth's Crust, Siberian Branch of the Russian Academy of Sciences, 128 Lermontov St, Irkutsk 664033, Russia

² Sobolev Institute of Geology and Mineralogy, Siberian Branch of the Russian Academy of Sciences, 3 Academician Koptuyug Ave, Novosibirsk 630090, Russia

³ Novosibirsk State University, 1 Pirogov St, Novosibirsk 630090, Russia

ABSTRACT. Linear or lens-like carbonate (marble) and carbonate-silicate bodies among gabbro and amphibolites within the Krestovsky subterrane of the Olkhon composite terrane (West Baikal Area) are identified as dikes. The dikes commonly dip almost vertically, range in thickness from 20 cm to a few meters, and are up to 100 m long. The Olkhon marble dikes quite often coexist with dolerite dikes and/or granite veins and show signatures of emplacement synchronously with the igneous bodies. The marble dikes differ from mantle carbonatites in mineralogy and chemistry and thus may be derived from sedimentary carbonate rocks molten during collisional events.

The origin of the Olkhon carbonate and carbonate-silicate dikes may be explained with two possible geodynamic scenarios. They may be derived either from Neoproterozoic carbonate sediments upon the Early Precambrian basement of a cratonic block which was involved in collisional events, or from abundant carbonate sedimentary material in an island-arc terrane. Large-scale melting of silicate and carbonate rocks was maintained by heat released from mantle mafic magma intruding into the lower crust. The batches of both crustal (carbonate and granitic) and mantle (mafic) melts intruded late during the collision in a strike-slip tectonic setting.

KEYWORDS: marble dike; Olkhon terrane; strike-slip tectonics; metamorphism; deformation

FUNDING: The research was supported by the Russian Foundation for Basic Research (grant 20-05-00005), and by the Russian Science Foundation (Project 18-17-00101), and by the Government of the Russian Federation (grant 075-15-2019-1883).

RESEARCH ARTICLE

Received: May 17, 2022

Revised: May 28, 2022

Accepted: June 14, 2022

Correspondence: Eugene V. Sklyarov, skl@crust.irk.ru

FOR CITATION: Sklyarov E.V., Lavrenchuk A.V., Mazukabzov A.M., 2022. Marble Dikes in the Olkhon Composite Terrane (West Baikal Area). *Geodynamics & Tectonophysics* 13 (5), 0667. doi:10.5800/GT-2022-13-5-0667

1. INTRODUCTION

Most of carbonate rocks in the crust are of sedimentary origin, while igneous carbonatites and metasomatic carbonate rocks of various compositions constitute less than 1 vol. % of the total carbonate budget. Carbonates differ markedly from coexisting silicate rocks in appearance and chemistry and thus make marker beds providing reliable reference in geological, tectonic, and paleogeodynamic reconstructions for complexly structured orogenic areas. The role of carbonate rocks in the understanding of local geology is especially important in areas of high-grade metamorphism where silicate rocks have lost their original texture and structure signatures and can only be interpreted proceeding from geochemistry. Carbonate bodies of different sizes within Precambrian cratons and metamorphic terranes commonly preserve their original stratigraphic position, but sometimes carbonates, which are more ductile than silicates, become extruded during rapid high-temperature synmetamorphic deformation and thus detach from their deposition place. Such displaced carbonate bodies are especially prominent in the Olkhon composite terrane in the western Baikal area where they occur as marble mélangé [Fedorovsky et al., 1993; Sklyarov et al., 2021] or marble "layers" [Sklyarov et al., 2013, 2021]. However, the allochthonous origin has been commonly doubted for

the Olkhon marble mélangé interpreted rather in terms of boudinage and local disintegration of abundant silicate rocks, and still more for the elongate marble bodies free from silicate fragments. This study continues our previous work on carbonate and carbonate-silicate rocks [Sklyarov et al., 2013] and marble mélangé [Sklyarov et al., 2021] in the Olkhon terrane. Here we focus on new details concerning carbonate and carbonate-silicate dikes, with implications for their origin.

2. OLKHON TERRANE: GEOLOGICAL BACKGROUND

Geology and tectonics of the Olkhon terrane have been largely studied, mainly by V.S. Fedorovsky and his colleagues from Moscow, St. Petersburg, Novosibirsk, and Irkutsk [Fedorovsky et al., 1995, 2017, 2020; Fedorovsky, Sklyarov, 2010; Sklyarov, 2005; Donskaya et al., 2017; etc.]. Therefore, we confine ourselves to a brief synopsis and issues relevant for the present study.

The Olkhon terrane is a part of the Early Paleozoic Baikal collisional belt [Donskaya et al., 2000] that delineates the Siberian craton in the south (Fig. 1). In the first approximation, it comprises two major units characterized previously as metamorphic volcanosedimentary complexes [Pavlovsky, Eskin, 1964; Eskin et al., 1979]: (i) Krestovsky subterrane composed mainly of marble, amphibolite, and

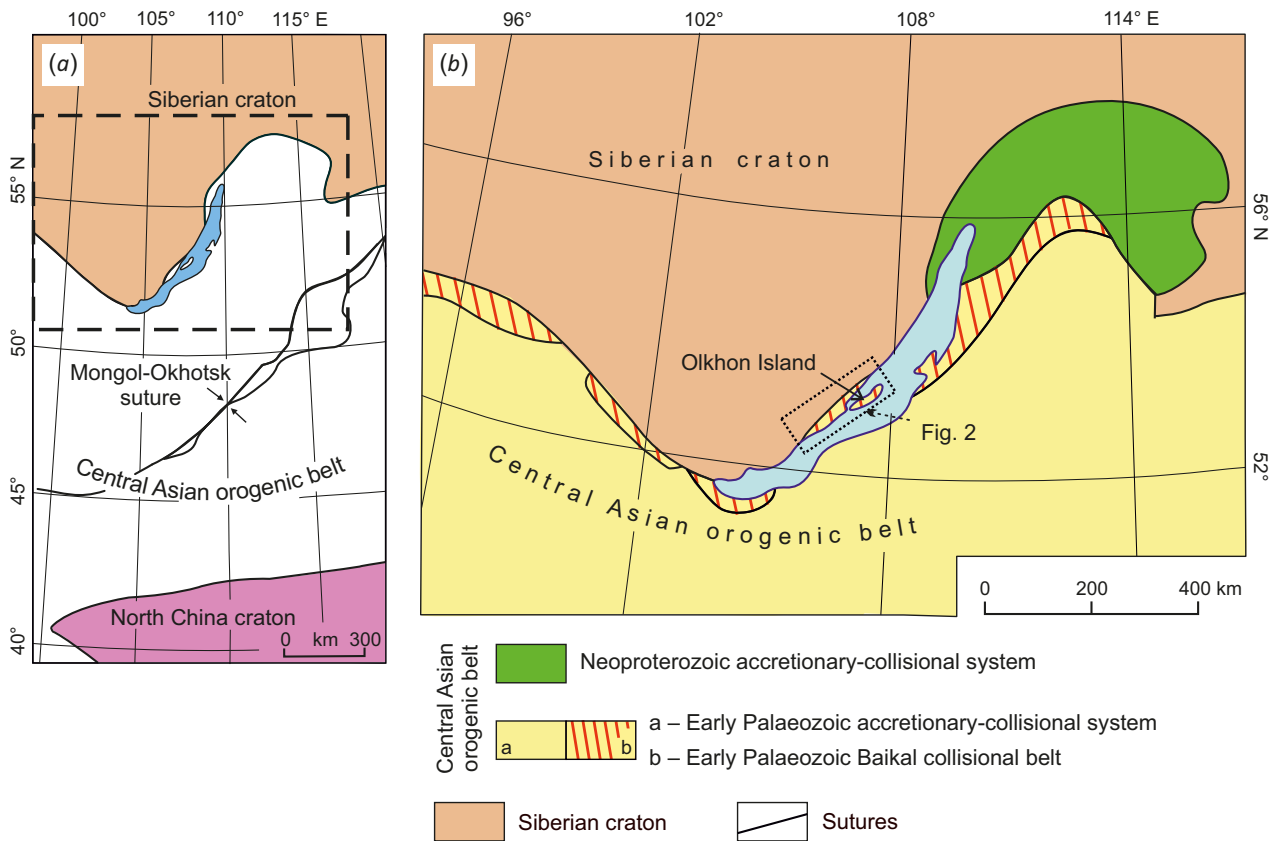


Fig. 1. Simplified tectonics of Central Asia (a) and metamorphic terranes in the Early Palaeozoic Baikal collisional belt of northern CAOB (b) modified after [Donskaya et al., 2017].

gabbro of the Birkhin volcanoplutonic complex making up >50 % [Gladkochub et al., 2014; Lavrenchuk et al., 2019]; (ii) a collage of several large blocks derived from protoliths of different ages and settings in the remaining part of the Olkhon terrane [Donskaya et al., 2017].

The well documented rocks of the terrane formed in the Early Paleozoic during several tectonic events: early thrusting, two later orogenic phases, and final strike-slip faulting associated with microcontinent-island arc and microcontinent-continent collisions [Sklyarov, 2005]. The large-scale strike-slip faulting produced lithologically, morphologically, and structurally different shear zones and shaped up the tectonic framework of the Olkhon area.

Carbonate (calcitic, dolomite-calcitic, and dolomitic marbles) and carbonate-silicate rocks occupy about 20 vol. % of the total Olkhon collisional zone (Fig. 2). Marbles often occur as relatively thin (10–100 m) kilometers long sheets, which were thought to be a slightly deformed succession of metamorphosed volcanosedimentary rocks. However, the apparent simplicity of the succession obviously contradicts the structural data and the presence of numerous shear zones mapped in the area to a high resolution [Fedorovsky, Sklyarov, 2010]. Carbonates often form "mixtures" with amphibolites or granulites in irregularly shaped zones and thus may be of exotic origin [Sklyarov et al., 2009, 2013, 2021].

3. MATERIALS AND METHODS

The dikes were examined, photographed, and sampled in coastal outcrops during winter campaigns, from frozen Lake Baikal; some sites were mapped at a scale of 1:5000, on the basis of satellite images.

Major elements were determined by the XRF analysis at the Center for Geodynamics and Geochronology of the Institute of the Earth's Crust (Irkutsk, Russia).

More than 300 grains of clinopyroxene, garnet, titanite, calcite, dolomite, epidote, and other coexisting minerals were analyzed in polished thin sections, at the Centre "Geospectr" of the Geological Institute SB RAS (Ulan-Ude, Russia). The analyses were performed by scanning electron microscopy with energy dispersive X-ray spectroscopy (SEM-EDS) on a LEO 1430VP scanning electron microscope equipped with an Oxford INCAEnergy 350 spectrometer, at the Geological Institute SB RAS. The operation conditions were 20 keV accelerating voltage, 0.3–0.4 nA beam current, <0.1 μm beam diameter, and 50 s counting time.

The results were checked against synthetic compounds and natural minerals: SiO (O, Si), BaF₂ (F, Ba), NaAlSi₃O₈ (Na), MgCaSi₂O₆ (Mg, Ca), Al₂O₃ (Al), Ca₂P₂O₇ (P), KAlSi₃O₈ (K), Cr-met. (Cr), Mn met. (Mn) and Fe met. (Fe). Matrix correction was performed with the XPP algorithm as part of the built-in Inca Energy software.

The analytical results are summarized in App. 1, Tables 1.1, 1.2, 1.3, 1.4.

4. CARBONATE AND CARBONATE-SILICATE DIKES

Carbonate dikes were found mainly within the Krestovskiy subterrane (Fig. 2) among gabbro and amphibolites, mostly in eroded coastal cliffs. The perfect exposure in the coastal cliffs allowed detecting and identifying the gabbro-hosted dikes as intruded bodies, unlike the partly buried dikes in gabbro where sporadic outcrops of carbonates can be misinterpreted as xenoliths, and especially unlike the dikes in amphibolites aligned with the host gneissic texture and looking like sedimentary beds.

There are four sites restricted to the Krestovskiy subterrane where dikes and dike swarms are located in different hosts (Fig. 2): amphibolites derived from the Ulan-Nur gabbro of the Birkhin complex (Ulan-Nur site, 1 in Fig. 2); amphibolites on the northeastern periphery of the Birkhin

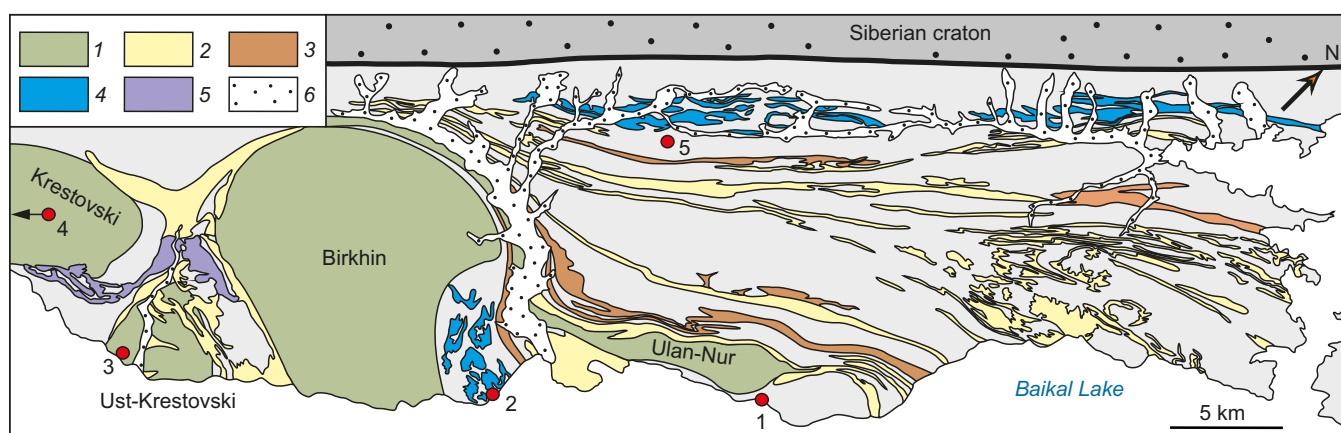


Fig. 2. Carbonate rocks in the central Olkhon terrane, modified after [Sklyarov et al., 2021].

1 – gabbro of the Birkhin (Krestovskiy, Birkhin, Ulan-Nur massifs) and Ust-Krestovskiy (Ust-Krestovskiy massif) complexes; 2 – calcite marble; 3 – dolomitic and calcite-dolomitic marbles; 4 – injection mélange; 5 – metamorphic lens-type mélange; 6 – Quaternary alluvium. Red circles are Ulan-Nur (1), Begul (2), Ust-Krestovskiy (3), Buguldeyka (4), and Tomota (5) sites.

gabbro complex, in the Anga – Begul interfluve (Begul site, 2 in Fig. 2); Ust'-Krestovsky gabbro (Ust'-Krestovsky site, 3 in Fig. 2); Buguldeika gabbro, Birkhin complex (Buguldeika site, southeast of the map in Fig. 2). In the remaining part of the Olkhon terrane, no evident marble or calc-silicate dikes have been observed, though some carbonates may be heavily deformed dikes, such as those from the Tomota site (5 in Fig. 2) mapped using GPS survey.

4.1. Ulan-Nur site

Several carbonate-silicate linear bodies in the Ulan-Nur site occur among amphibolites derived from the Birkhin gabbro. Two bodies obviously look like dikes, while the others bear signatures of ductile deformation and can be either dikes or xenoliths in gabbro. One nearly vertical carbonate-silicate dike, 20 cm to 1.5 m thick (Fig. 3, a), has its central thickest part composed of banded fine material,

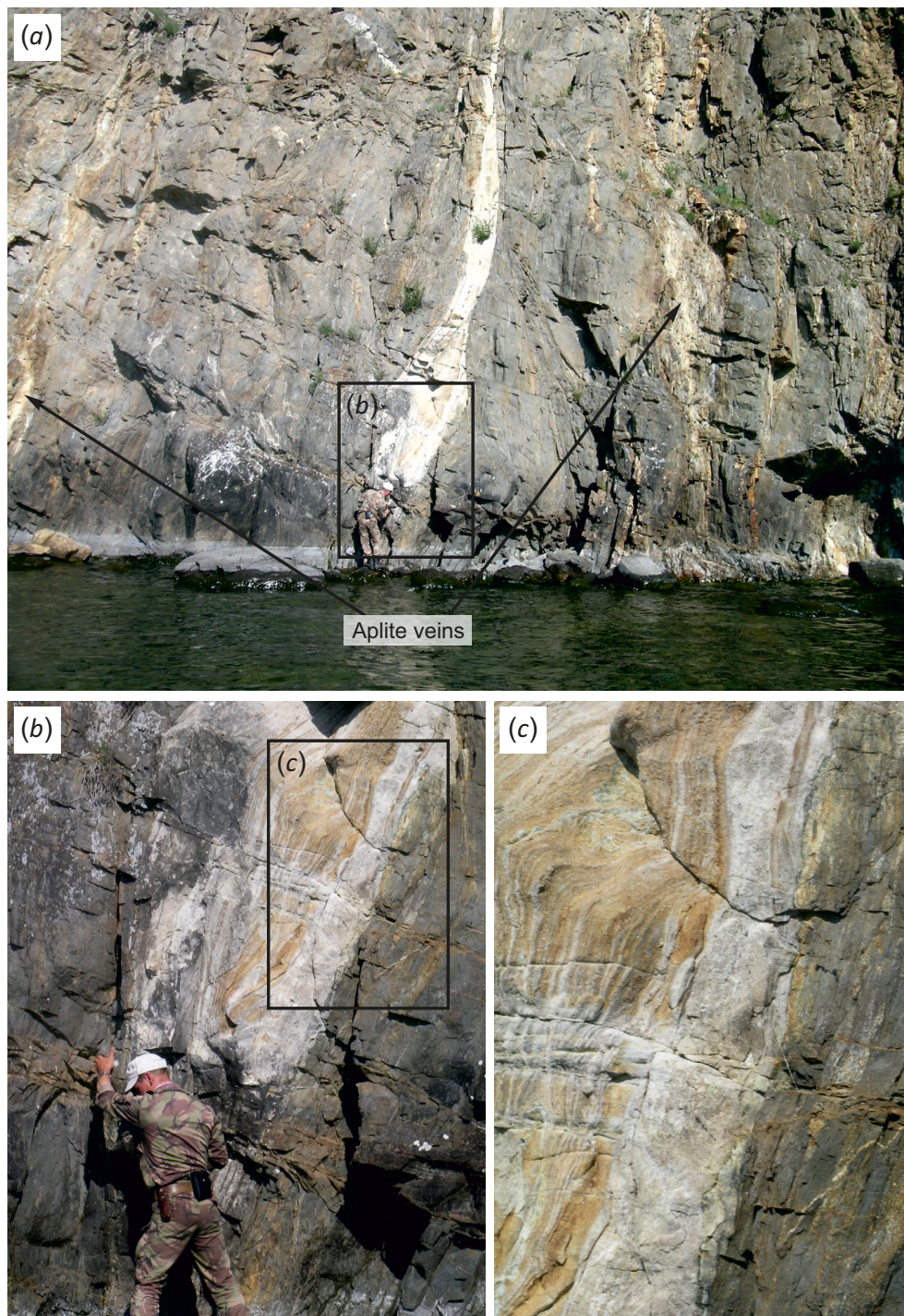


Fig. 3. Carbonate-silicate dike in amphibolite derived from the Ulan-Nur gabbro. (a) – general view; (b, c) – enlarged fragments (sample 09A160).

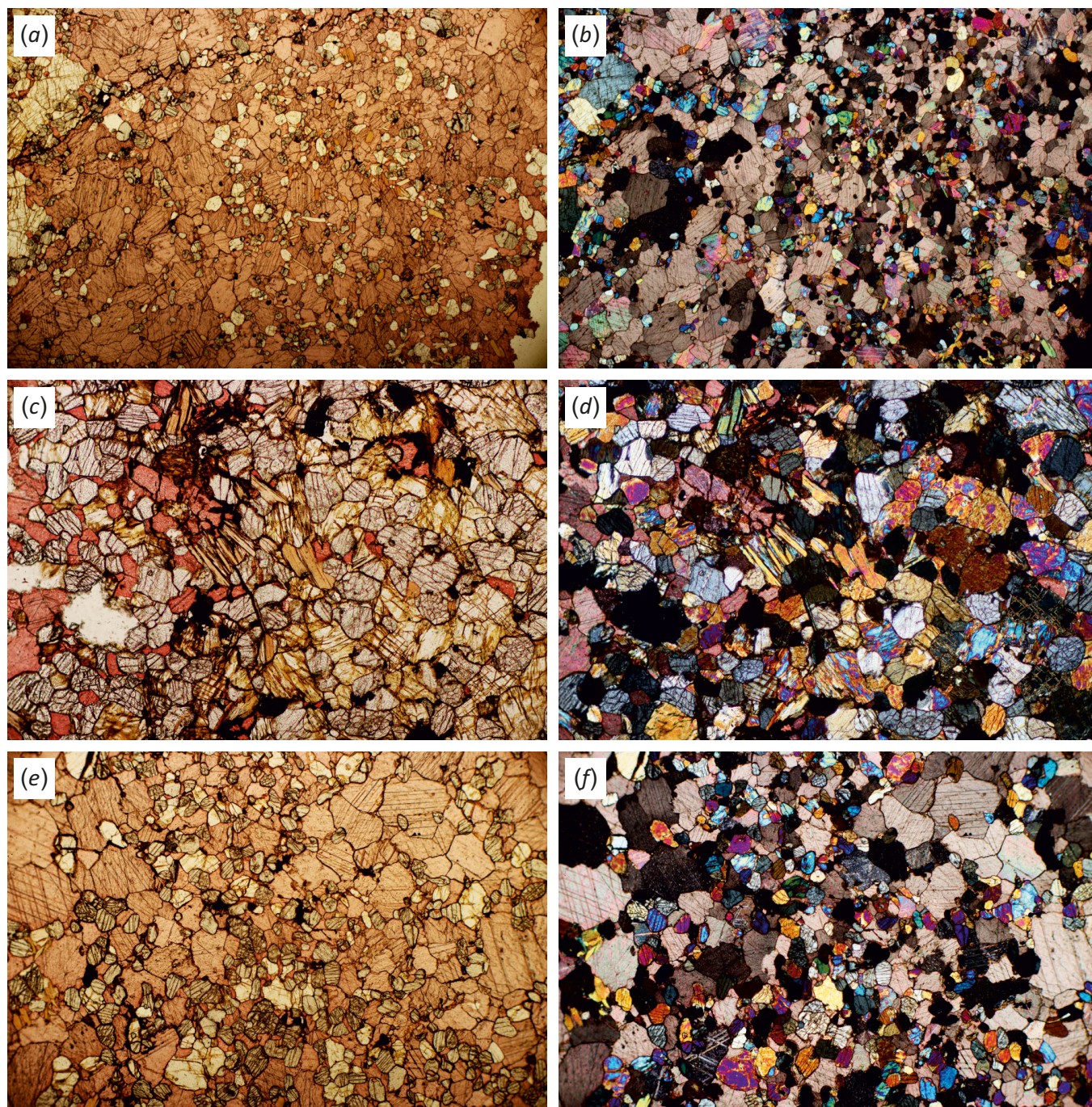


Fig. 4. Photomicrograph of thin sections from carbonate-silicate dike (sample 09A160). (a, b) – carbonate-silicate rock from dike center; (c, d) – skarn-like fragment from dike center; (e, f) – carbonate-silicate rock from dike margin. Samples 09A160A (a–d) and 09A160B (e, f). Reddish staining of calcite in the thin sections is due to alizarin paint. The images are in plane-polarized (a, c, e) and cross-polarized (b, d, f) light. See text for other explanations.

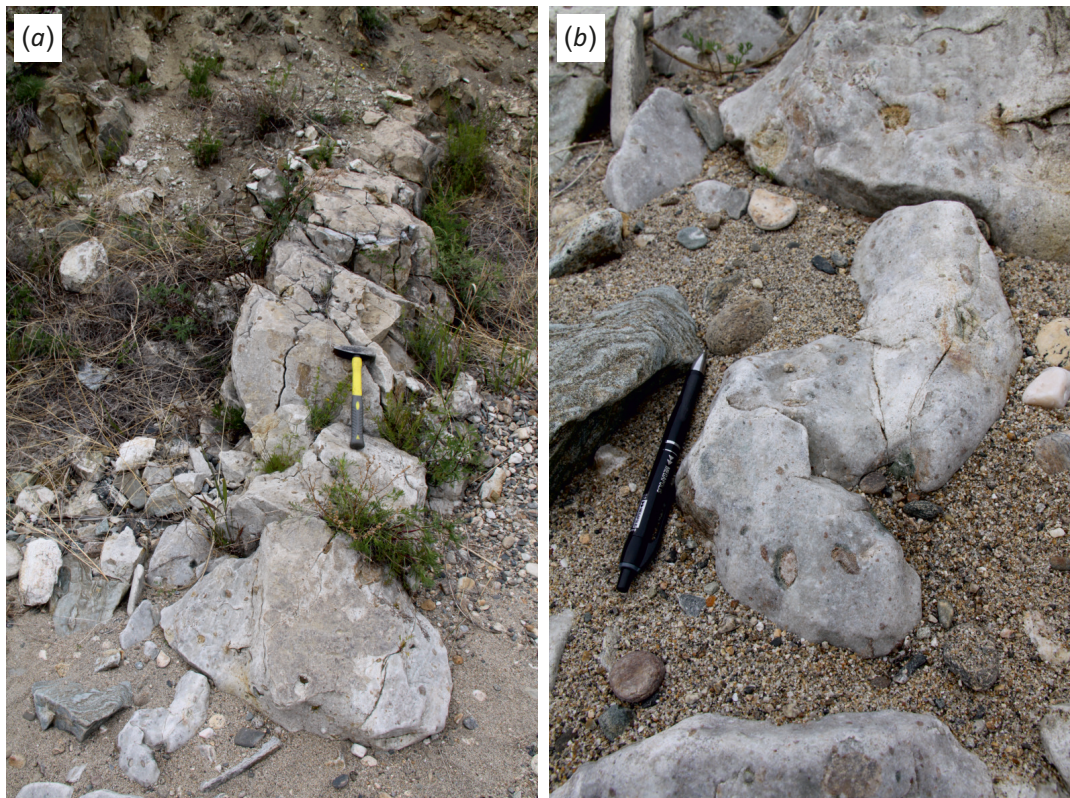


Fig. 5. Carbonate-silicate dike with large skarn fragments, mainly composed of garnet and pyroxene (sample SE542E). (a) – general view of outcrop; (b) – enlarged fragment with numerous skarn patches. See text for explanation.

yellowish on the surface, with alternated carbonate and silicate bands containing 10–20 vol. % of silicate minerals (Fig. 3, b, c). The dike has white massive margins (up to 30 cm) where calcite and iron-free silicate minerals are hard to discriminate. The dike generally strikes along the gneissic texture (foliation) of amphibolites but locally truncates it at a high angle. The outcrop also exposes aplite veins sub-parallel to the carbonate-silicate dike. The mineralogy of the dike consists of calcite, fine diopside, and scapolite (Fig. 4, a, b), as well as rare large skarn-like fragments composed of coarse K-feldspar crystals, fine scapolite grains (often round), fine diopside, sporadic grains of phlogopite and quartz, minor amounts of calcite (Fig. 4, c, g), and graphite occupying the interstitial space or rarely coating calcite grains.

The carbonate-silicate rocks of the margin have inequigranular textures, with patches of coarse calcite and small percentages of other minerals. The mineral assemblage includes ubiquitous fine anhedral scapolite and diopside, as well as fine graphite that locally fills cracks in calcite and scapolite (Fig. 4, d, e), or fills irregular cracks and coats grains of other minerals in phlogopite-rich linear zones. Rare phases are quartz, possibly forsterite, as well as zircon or titanite with high birefringence.

The other dike, varying in thickness from 0.5 m to 1 m, is partly buried and lies among banded carbonate-silicate

rocks (Fig. 5, a). It differs from the first dike in the presence of numerous skarn-like fragments, up to 10 cm, with diverse mineralogy: diopside and garnet of variable relative percentages (Fig. 5, b), ubiquitous K-feldspar, epidote, and titanite, locally occurring in clusters (Fig. 6, e, f), less frequent plagioclase and allanite, as well as fine ($\leq 20 \mu\text{m}$) zircon. The calcite matrix encloses quite numerous euhedral garnet, pyroxene, and titanite (Fig. 6, a, b, c, d).

Silicate minerals, both within the skarn fragments and individual crystals, show highly variable compositions. All garnets belong to the grossular-andradite series, with minor to absent spessartite, almandine, and pyrope components (App. 1, Table 1.1). The grossular component predominates and even locally approaches 100 %, while andradite reaches 39 % with as low as 2 wt. % TiO_2 . Pyroxenes are of diopside type containing ≤ 10 wt. % FeO (App. 1, Table 1.2), while more ferrous varieties (up to 21 wt. % FeO) are very rare. Allanite is zoned, with higher REE contents in the rim. Total REEs (limited to LREE La, Ce, Pr, and Nd) range from 7 to 20 wt. % (App. 1, Table 1.3). K-feldspar contains up to 4.3 wt. % BaO (App. 1, Table 1.4).

4.2. Begul site

Several nearly vertical marble dikes of various shapes and structure patterns, from 0.3 m to 1.5 m thick, occur in coastal cliffs near the Anga River mouth in amphibolites

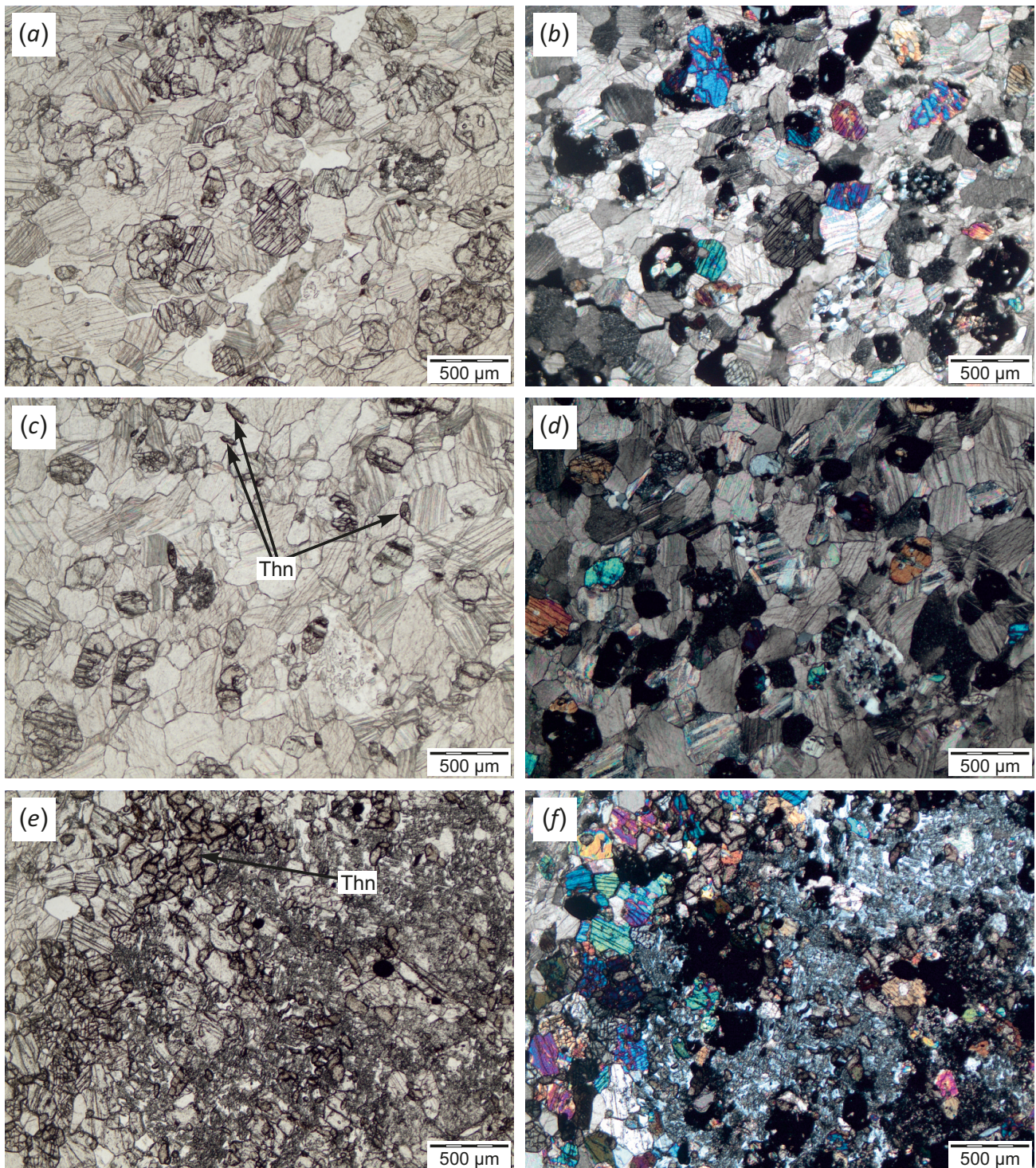


Fig. 6. Photomicrograph of thin sections of carbonate-silicate rock (*a-d*) and skarn fragment (*e, f*) from dike (sample SE542E). (*a, b*) – crystals of garnet and pyroxene in a calcite matrix; (*c, d*) – crystals of garnet and pyroxene, as well as fine spindle-shaped titanite in a calcite matrix; (*e, f*) – skarn fragment composed of pyroxene, garnet, and K-feldspar with fine titanite.

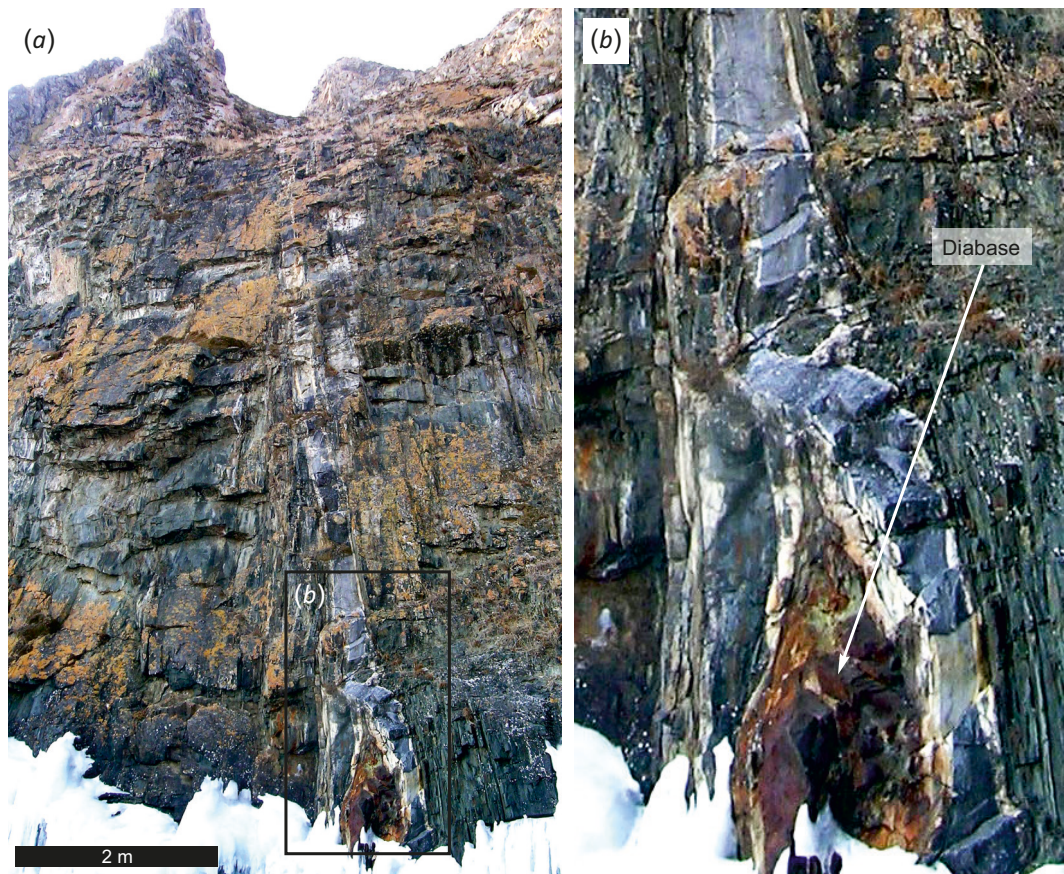


Fig. 7. Dike of calcite marbles in amphibolites derived from the Begul gabbro (a) and its enlarged fragment showing white "chilled margins" (b).

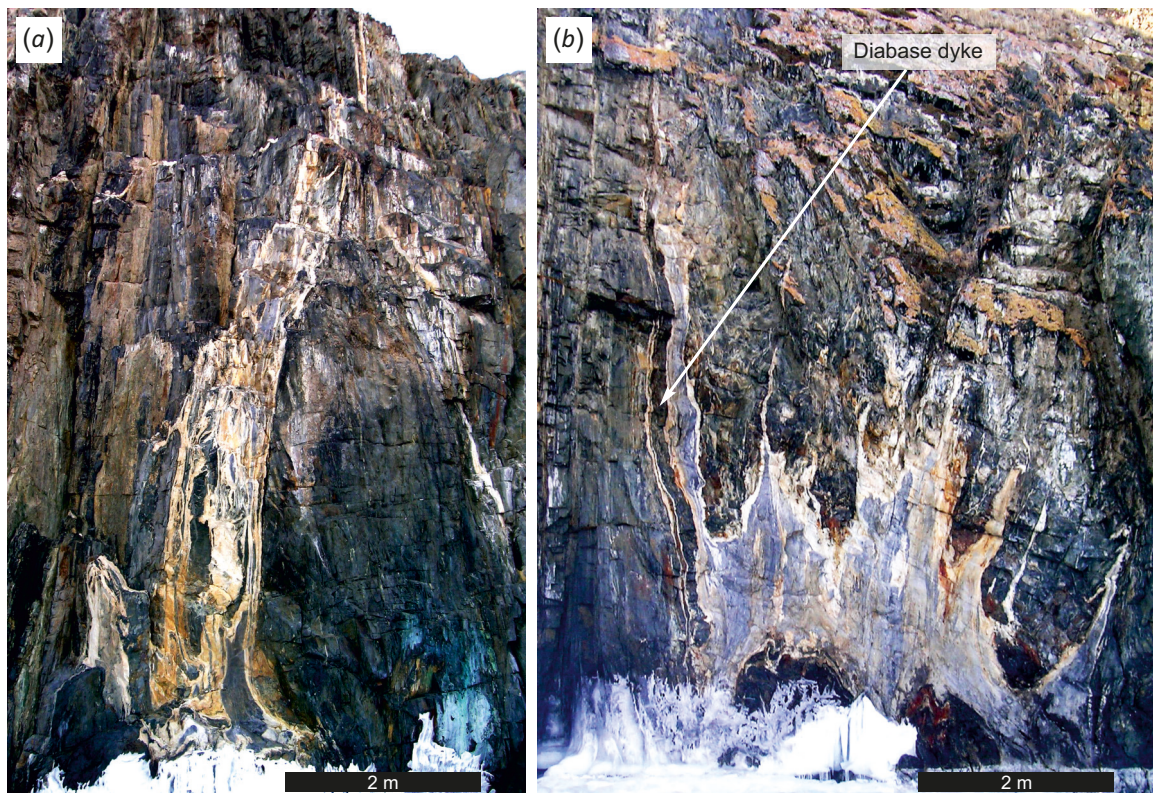


Fig. 8. Mottled (a) and irregularly shaped (b) dikes of calcite marble in amphibolites derived from the Begul gabbro.

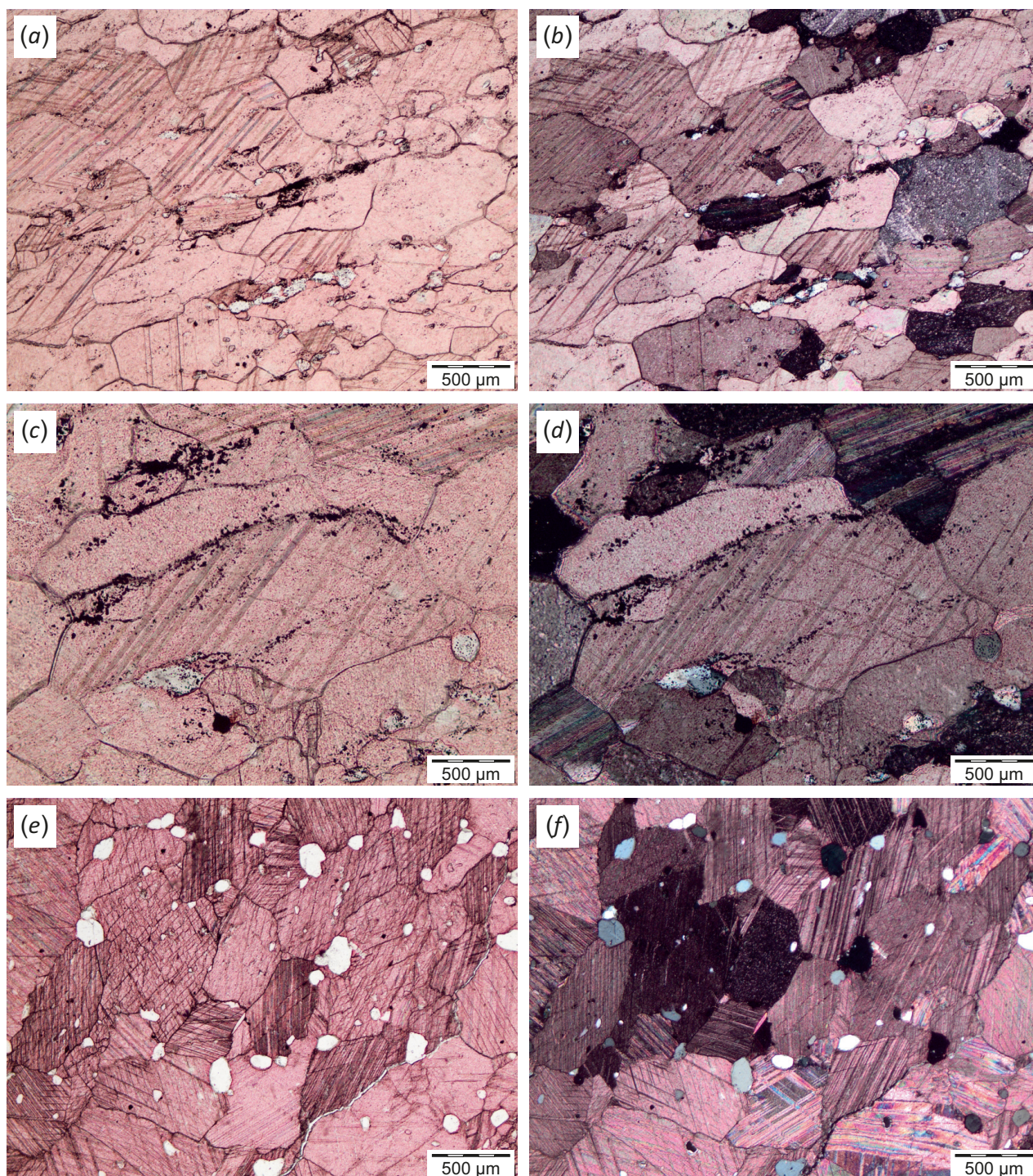


Fig. 9. Photomicrograph of polished thin sections of a zoned calcitic marble dike (sample SE1152). (a, b) – calcitic marble with quartz lenses in the dike center; (c, d) – linear zones impregnated with graphite in the dike center; (e, f) – calcitic marble enclosing quartz grains in the dike margin. Reddish staining of calcite in the thin sections is due to alizarin paint. The images are in plane-polarized (a, c, e) and cross-polarized (b, d, f) light.

derived from the Begul gabbro. The simplest dike (Fig. 7) is composed of dark gray fine calcite marble and has 3 to 10 cm thick white margins ("quench zones").

Some dikes, also with white margins, are of more intricate shapes (Fig. 8), possibly because of syndeformation emplacement. One such dike looks mottled due to alternating dark gray and white marble varieties (Fig. 8, a) and another one coexists with a thin dike of metadolerite (Fig. 8, b).

The mineralogy of the dikes is quite simple: fine calcite with unevenly distributed bands or elongate lenses of quartz, or rarely plagioclase, with few phlogopite flakes (Fig. 9, a, b). The dark gray color of the marble is due to the presence of disseminated graphite along or sometimes across grain boundaries of calcite (Fig. 9, b, d). Marble in the white margins contains slightly greater percentages of quartz and encloses larger and more sporadic graphite grains, often of a hexagonal habit. Quite many quartz grains look euhedral (Fig. 9, e, f).

4.3. Ust'-Krestovsky site

A swarm of numerous marble dikes, up to 500 m long and 0.5 to 10 m thick (Fig. 10), oriented roughly parallel to

the gabbro-granite contact, was mapped on the periphery of the 460–470 Ma Ust'-Krestovsky subalkaline gabbro [Lavrenchuk et al., 2017]. The carbonate dikes coexist with calc-silicate and rarer granite veins, as well as with few dolerite dikes; the carbonate and igneous dikes strike in the same direction. One relatively thick and long dike encloses banded or mottled skarn fragments, from few tens of cm to 1.5 m in size, with garnet-pyroxene-wollastonite-zoisite (Fig. 11, a, b) or wollastonite-zoisite-plagioclase-pyroxene (Fig. 11, c) mineralogy. Judging by their contact with the host gabbro (either direct or via an intermediate marble layer), the skarn blocks originated in a deep level and were then exhumed together with extruding marble and carbonate-silicate material. This hypothesis is consistent with different orientations of skarn structures produced by alternating mostly pyroxene and wollastonite-zoisite bands (Fig. 11, b).

Some carbonate-silicate dikes enclose irregularly shaped dikes of pyroxene porphyrite (Fig. 12, a) or more rarely granite. The porphyrite dikes are in some cases split into blocks (Fig. 12, b). The contacts of dikes with the host gabbro are free from signatures of metasomatism. Most of the dikes are composed of calcitic marble with minor amounts

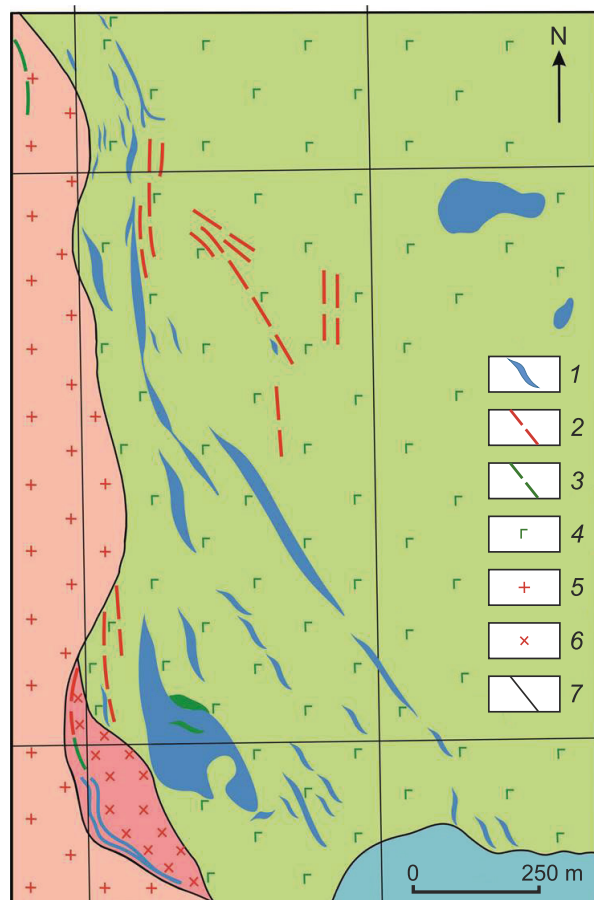


Fig. 10. Marble and calc-silicate dikes in the Ust-Krestovsky gabbro (sample SE1507), after [Sklyarov et al., 2021]. 1 - marble and calc-silicate dikes; 2 - granite veins; 3 - dolerite dikes; 4 - gabbro; 5 - granite; 6 - diorite; 7 - geological boundaries.

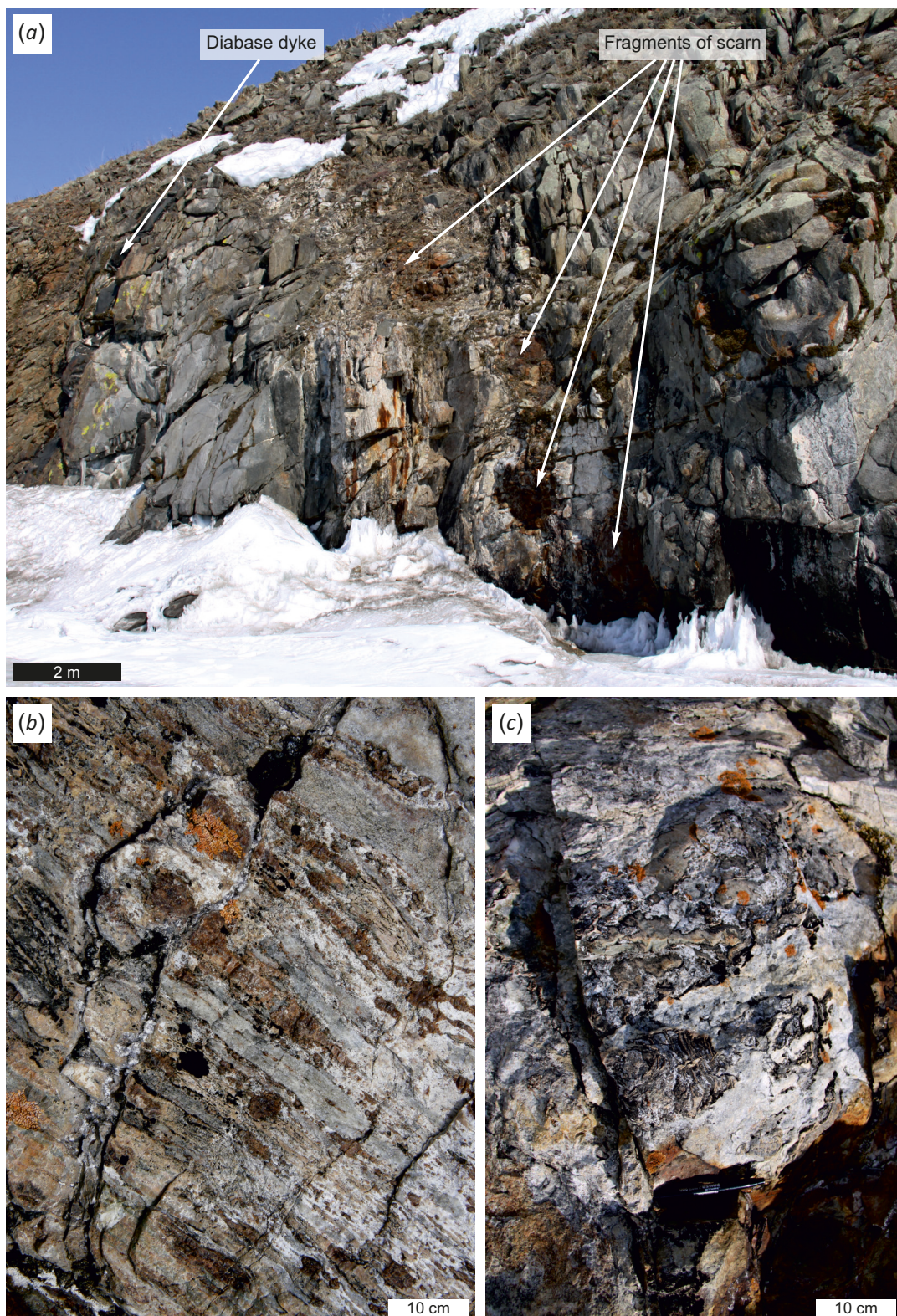


Fig. 11. Dike of calcitic marble with skarn fragments in the Ust'-Krestovsky gabbro. (a) – general view of calcitic marble dike and dolerite dike on the left; (b) – fragment of banded skarn composed of mainly of garnet (brown), pyroxene (greenish-grayish), and calcite (white); (c) – fragment of mottled skarn blocks of wollastonite-zoisite-plagioclase composition.

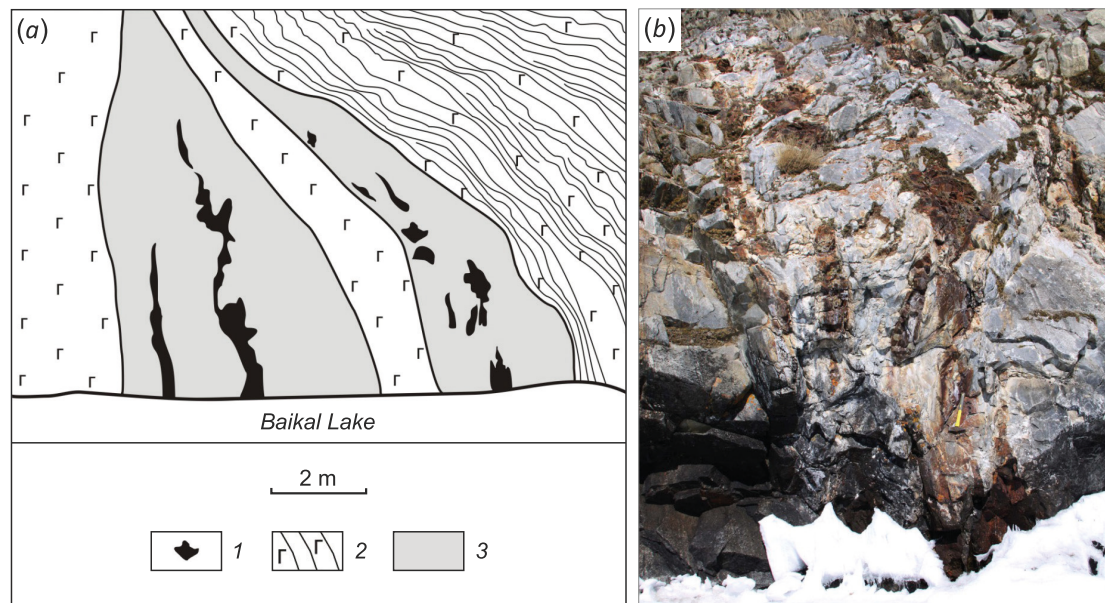


Fig. 12. Marble dikes coexisting with dolerite in the Ust-Krestovsky gabbro.

(a) – photograph-based sketch, (b) – photograph, after [Sklyarov et al., 2021]. 1 – dolerite; 2 – gabbro with magmatic layering; 3 – fine-grained marble. (a) – two blind dolerite dikes in marble (left) and dolerite fragments in marble (right); (b) – reddish-brown dolerite fragments in marble (right part of sketch).

of silicate minerals. The minerals of carbonate-silicate rock and skarn show variable chemical compositions (App. 1, Tables 1.1, 1.2, 1.3, 1.4).

4.4. Buguldeika site

Carbonate dikes in the Buguldeika gabbro were studied at two sites of white massive calcitic marble and dolomitic marble, respectively. The calcitic marble dikes are steep branching bodies, 30–70 cm thick, locally with angular xenoliths of the host gabbro (Fig. 13, a). The dike of white to pinkish fine dense dolomitic marble is traceable quasi-horizontally over a distance of 150 m and reaches a thickness of 2 m (Fig. 13, b). Its contacts with gabbro are often marked by ≤ 10 cm thick lenses of pyroxene-zoisite-plagioclase skarn (Fig. 13, c), while the marble is free from silicate minerals.

4.5. Tomota site

The Tomota site is located within a large shear zone composed of migmatized gneiss and granite-gneiss with abundant concordant pegmatite-aplite veins occupying more than 50 vol. % of all rocks [Fedorovsky et al., 2012]. The good exposure of the site allowed us to map calcitic marble and amphibolite bodies traceable as parallel chains of small lenses (Fig. 14) varying in size from ten to hundred meters long and 3 to 15 m thick. The host biotite and garnet-biotite gneisses are cut by numerous pegmatite-aplite veins from 30 cm to 7 m in thickness. Amphibolites, including garnet-bearing ones, have typical gneissic or locally massive textures and can be interpreted as meta-gabbro. Note

that neither carbonate nor igneous mafic bodies occur north and south of the site and farther along the gneissic sequence.

Carbonate bodies are almost pure fine to medium calcitic marbles, free from skarn at the contact with gneiss. Linear carbonate bodies, possibly, dikes, are known from other parts of the Olkhon terrane as well, e.g., in the Tazheran complex located near the Ulan-Nur site [Sklyarov et al., 2009, 2013], or in cliff exposures on the north-eastern tip of Olkhon Island. However, they may be interpreted in different ways according to structure and geometry.

5. DISCUSSION

The sampled marble and carbonate-silicate dikes have some key features. Their occurrence in the Olkhon terrane is not limited to the sampled sites. The abundant linear bodies in the area are sometimes hard to identify as dikes because they are commonly aligned with the gneissic texture of the silicate hosts and are often poorly exposed. Therefore, they have been rather misinterpreted as layers in a metamorphosed carbonate-silicate sequence. The sampled carbonate and carbonate-silicate dikes were detected due to perfect exposure in coastal cliffs (except for those from the Tomota site). The bodies from the Ust-Krestovsky and Buguldeika gabbro are obviously of dike origin, though it is tempting to attribute them to xenoliths despite the length-to-thickness ratios exceeding 100:1. The dikes in amphibolites can be reliably classified as such if they truncate the gneissic texture, as in the Ulan-Nur and Begul sites (see Figs. 7, 8). Another piece of evidence against the sedi-

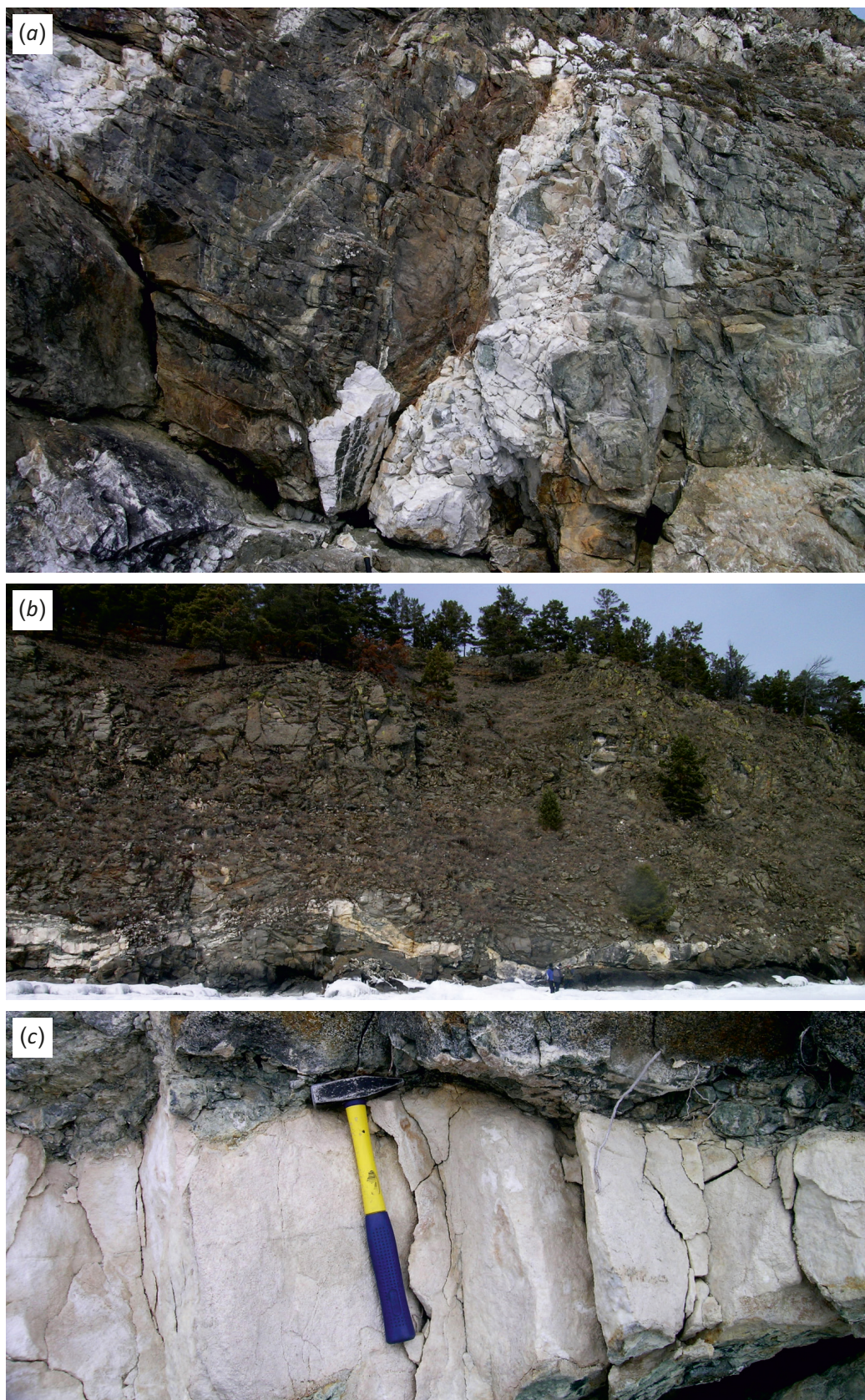


Fig. 13. Marble dikes in the Birkhin gabbro, Buguldeika site.

(a) – steep branching dikes of calcitic marble; (b) – nearly horizontal dike of dolomitic marble; (c) – fragment of dolomitic marble dike with pyroxene-zoisite-plagioclase skarn.

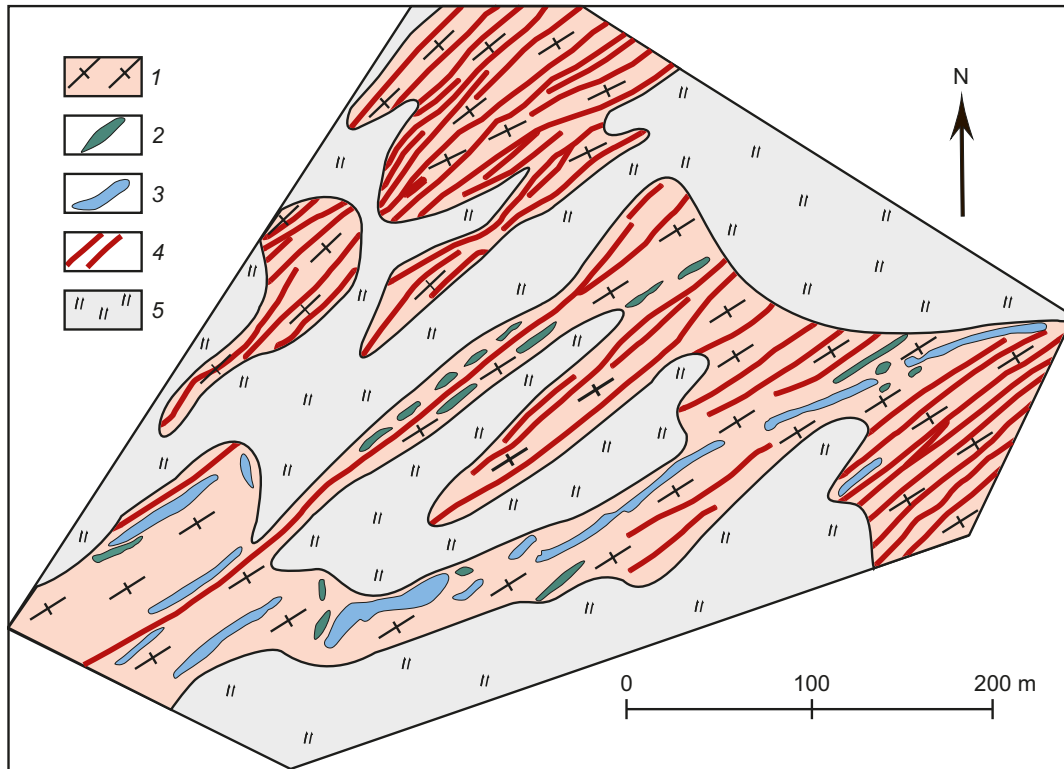


Fig. 14. Deformed dikes of calcitic marble and metagabbro among gneisses, Tomota site. 1 – biotite or less often garnet-biotite gneisses; 2 – metagabbro and amphibolite derived from gabbro; 3 – calcitic marble; 4 – granitic and pegmatite-aplitic veins; 5 – vegetated surface.

mentary origin of carbonates comes from the dike margins with greater percentages of quartz and lesser amounts of disseminated graphite (see Fig. 7). The formation mechanism of these zones remains unclear but it hardly can be sediment deposition anyway. It is very problematic to prove that the linear carbonate bodies among gneisses are dikes because the rocks of the terrane were heavily deformed by strike-slip shear, especially the least competent silicate igneous and sedimentary rocks. As a result of tectonic activity, the rocks became disintegrated and made chains of fragments, as in the Tomota site (Fig. 14), or were extruded ductily into larger bodies. The dike origin of such bodies is further supported by their co-occurrence with chains of metamorphosed mafic rocks, including metagabbro. Note in this respect that carbonate dikes from almost all sampled sites coexist either with metadolerites, as in the Begul site (see Fig. 7), or with granites, as in the case of Ulan-Nur (see Fig. 3), or with both, as in the Ust'-Krestovskiy site (see Fig. 12). Therefore, silicate and carbonate melts apparently intruded almost synchronously. However, it remains to clear up whether it was carbonate melt or viscoplastic flow.

Note that the sampled dikes hardly can be carbonatite intrusions because their compositions (App. 1, Table 1.5) mismatch the mineralogical and chemical features of mantle carbonatite [Bell, Tilton, 2002]. On the other hand, the

Olkhon carbonate-silicate rocks have typical skarn mineralogy (App. 1, Tables 1.1, 1.2, 1.3, 1.4), with the presence of zircon, allanite, and some other minerals easily explicable by interaction with granite or syenite melts. Melting in the carbonate-gneissic substrate of lower crust appears to be the only possible origin for the carbonate and carbonate-silicate melts of the Olkhon terrane. Melting of mantle carbonates requires temperatures above 1200 °C [Wyllie, Tuttle, 1960], which are not expected to exist in the crust according to the available evidence, though these temperatures may be workable for crust melting as well. Meanwhile, the dry and wet melting of silicates may begin at 200 to 300 °C different temperatures, in the same way as for carbonates, for which it was proven experimentally already long ago. Namely, melting of calcite at 1 kbar begins at 740 °C in the presence of an aqueous fluid [Wyllie, Tuttle, 1960] and at progressively lower temperatures to 600 °C if the pressures increase or if MgO is added to the system [Fanelli et al., 1986]. At a fixed composition of the fluid ($X_{CO_2} = 0.05$), the wet granite solidus roughly coincides with the calcite melting line and is 100 °C above that of dolomite one [Lentz, 1999]. The melting of the crust is only limited by water contents in the melting region. In the case of the carbonate-gneiss substrate of the Olkhon terrane, the presence of pegmatite-aplitic veins locally occupying more than 20–30 vol. % [Fedorovsky, Sklyarov, 2010], provides evidence

of wet melting, as their formation requires additional H_2O in the substrate [Patino Douce, Harris, 1998]. Direct crystallization of dikes from melt can be inferred from their massive structure free from traces of flow or brittle fracture, as well as from zoning with texture and composition difference between the central and margin zones (Ulan-Nur and Begul sites).

On the other hand, many carbonate-silicate dike rocks are composed of alternating bands with different relative percentages of silicate minerals and calcite, possibly, as a result of viscoplastic flow. Furthermore, their typically skarn mineralogy would cast doubt on the dike origin if the skarn mineral assemblages were considered to be solid proof for interaction of silicate melts with solid carbonate material. However, this evidence against the intrusion of a carbonate melt into a silicate matrix may be ambiguous: interaction of a hydrous carbonate melt with amphibolites or gabbro can lead to the same metasomatic reactions, while skarn does not follow the carbonate-silicate contacts but commonly occurs as quite large fragments (Ust'-Krestovsky site, see Fig. 11) or as clusters of euhedral garnet, pyroxene, and other skarn minerals in a silicate-carbonate matrix (Ulan-Nur site, see Fig. 5). The silicate-carbonate dikes may have shaped up during the crystallization with subsequent ductile flow of material in an active tectonic setting.

It still remains unclear whether the carbonate and carbonate-silicate material was molten or viscoplastic when emplacing in the silicate rocks of the Olkhon terrane. Melt inclusions would provide explicit evidence for direct crystallization, but no such inclusions have been detected and hardly can have survived after re-crystallization during later cooling. Silicates in the Olkhon dikes are apparently of metasomatic origin, which however does not contradict crystallization from a melt with subsequent metasomatism upon interaction with the carbonate and silicate components during cooling. For instance, silicate minerals in mantle-derived carbonatite from a calcite dike in Alnö Island were inferred [Vuorinen, Skelton, 2004] to originate by interaction of calcite melt with the wall rock.

Judging by coexistence of the Olkhon marble dikes with metadolerite dikes and granite veins, as well as by similar 460–470 Ma ages of the igneous rocks [Sklyarov, 2005; Fedorovsky et al., 2010], the origin of the carbonate and carbonate-silicate dikes (this study) and marble mélange among silicate complexes [Sklyarov et al., 2013, 2021] may be explained in terms of two possible geodynamic scenarios. One scenario implies carbonate deposition within an island arc terrane affected by a hot field [Yarmolyuk et al., 2013; Lavrenchuk et al., 2017]. According to this scenario, the hot field maintained heating of the whole system and induced melting of mafic magmas that left record as voluminous igneous rocks of the Birkhin and Ust'-Krestovsky

complexes. Heat transfer by mafic magma moving to the lower crust heated the crustal material thus increasing its plasticity and induced melting of granite and, possibly, carbonate, which rose together with the mafic magma. Such nearly synchronous intrusion likely produced granite, dolerite, carbonate, and mingling dikes.

In another scenario, amalgamation of the Olkhon collisional terrane and its accretion to the Siberian craton involved oceanic crust of a back-arc basin composed of ophiolites, sediments [Donskaya et al., 2017; Sklyarov et al., 2020], island arc complexes, and a cratonic block with an Early Precambrian basement and Neoproterozoic passive margin sediments, mostly of carbonate lithologies. The Precambrian cratonic block may be a fragment detached from Siberia (judging by the presence of Neoproterozoic carbonates in its neighbor parts) or from some other craton. It may have moved to the lower crust where it underwent heating and partial melting in the thickened crust during a collision event, with an additional effect of mantle mafic melts in the presence of an aqueous fluid and the ensuing formation of granite and carbonate melts. Then batches of granitic and carbonate crustal and mafic mantle melts were intruded pulse-like into the upper crust to produce the mosaic observed on the surface. Yet, at the time being, the authors have different opinions about the preferable scenario.

Carbonate dikes are not specific to the Olkhon terrane. Thin dikes of calcite marble among amphibolites were reported [Roberts, Zwaan, 2007] from one of higher nappes in the Caledonides of Troms, northern Norway. The dikes were inferred [Roberts, Zwaan, 2007] to have intruded at the final deformation stage of the Scandian orogeny (strike-slip motions during orogen collapse). Furthermore, swarms of carbonatite-like dikes, with typical metamorphic mineralogy (forsterite, spinel, pargasite, scapolite, etc.), occur in granulite facies gneisses of the Greater Himalayan Crystalline sequence in the collisional system of the Eastern Himalayan syntaxis [Liu et al., 2006]. More evidence of crustal carbonate melts comes from Paleoproterozoic crustally derived carbonate-rich magmatic rocks from the Daqinshan area, North China Craton, where numerous carbonate-silicate bodies, termed "crustal carbonatite", are nearly coeval to granulite metamorphism of the host gneisses [Wan et al., 2008]. There are other known examples of marble dikes, and their geography may extend in the nearest future.

6. CONCLUSION

Dikes of calcitic and dolomitic marbles and carbonate-silicate rocks within the Olkhon terrane are reliably identifiable only in gabbro and amphibolites of the Krestovsky subterrane. However, the linear or lens-shaped carbonate bodies among gneisses elsewhere in the terrane may be problematic to identify as dikes because the protolith

sedimentary or felsic to intermediate igneous rocks were involved in large-scale strike-slip related shearing. Most of the dikes dip nearly vertically but some have shallow dips. They vary in thickness from 20 cm to a few meters and are traceable to distances over 100 m. The carbonate dikes often coexist with roughly coeval dolerite dikes and/or granite veins. The dikes differ markedly from mantle-derived carbonatite in mineralogy and chemistry and may have formed by melting of sedimentary rocks during collisional events. The silicate-carbonate dikes have typical skarn mineralogy (grossular-andradite garnet, diopside-hedenbergite clinopyroxene, wollastonite, titanite, zoisite-clinozoisite, K-feldspar, etc.) resulting from interaction of carbonate and silicate material during the system cooling.

The suggested model implies heating associated with upward motion of mafic mantle magmas and the ensuing large-scale melting of silicate granitic rocks and carbonates in the thickened lower crust. Batches of granitic and carbonate melts, as well as mantle mafic magmas, emplaced in a setting of active strike-slip tectonism. The protolith of sedimentary carbonates that intruded into the silicate matrix as dikes or marble *mélange* can be explained in two ways: (i) volcanic-sedimentary deposits in a Early Paleozoic island arc; (ii) part of a cratonic block, with an Early Precambrian basement and Neoproterozoic carbonate sediments, which was involved into collision.

The carbonate and silicate-carbonate dikes of the Olkhon composite terrane are of rare but not unique occurrence. Such dikes were reported from a nappe of Caledonides in Norway [Roberts, Zwaan, 2007], a Crystalline sequence in the eastern Himalayan syntaxis [Liu et al., 2006], Paleoproterozoic metamorphics in the North China craton [Wan et al., 2008], and some other metamorphic complexes worldwide.

7. ACKNOWLEDGEMENT

We wish to thank O.A. Sklyarova and I.G. Barash for assistance with figures. The manuscript profited from constructive criticism by A.N. Didenko and A.A. Sorokin, Corresponding Members of the Russian Academy of Sciences.

8. CONTRIBUTION OF THE AUTHORS

The authors contributed equally to this article.

9. CONFLICT OF INTERESTS

The authors have no conflicts of interest to declare. All authors have read and agreed to the published version of the manuscript.

10. REFERENCES

Bell K., Tilton G.R., 2002. Probing the Mantle: The Story from Carbonatites. *Eos* 83 (25), 273–277. <https://doi.org/10.1029/2002EO000190>.

Donskaya T.V., Gladkochub D.P., Fedorovsky V.S., Sklyarov E.V., Cho M., Sergeev S.A., Demonterova E.I., Mazukabzov A.M., Lepekina E.N., Cheong W., Kim J., 2017. Pre-Collisional (>0.5 Ga) Complexes of the Olkhon Terrane (Southern Siberia) as an Echo of Events in the Central Asian Orogenic Belt. *Gondwana Research* 42, 243–263. <https://doi.org/10.1016/j.gr.2016.10.016>.

Donskaya T.V., Sklyarov E.V., Gladkochub D.P., Mazukabzov A.M., Sal'nikova E.B., Kovach V.P., Yakovleva S.Z., Berezhnaya N.G., 2000. The Cisbaikal Collisional Metamorphic Belt. *Doklady Earth Sciences* 374 (7), 1075–1079 (in Russian) [Донская Т.В., Склярлов Е.В., Гладкочуб Д.П., Мазукабзов А.М., Сальникова Е.Б., Ковач В.П., Яковлева С.З., Бережная Н.Г. Прибайкальский коллизионный метаморфический пояс // Доклады РАН. 2000. Т. 374. № 7. С. 1075–1079].

Eskin A.S., Ez V.V., Grabkin O.V., Letnikov F.A., Melnikov A.B., Morozov Yu.A., Shkandry B.O., 1979. Correlation of Deep-Seated Processes in the Precambrian Metamorphic Complexes of the Baikal Area. *Nauka, Novosibirsk*, 118 p. (in Russian) [Ескин А.С., Эз В.В., Грабкин О.В., Летников Ф.А., Мельников А.И., Морозов Ю.А., Шкандрий Б.О. Корреляция эндогенных процессов в метаморфических комплексах докембрия Прибайкалья. Новосибирск: Наука, 1979. 118 с.].

Fanelli M.T., Cava N., Wyllie P.J., 1986. Calcite and Dolomite without Portlandite at a New Eutectic in CaO–MgO–CO₂–H₂O with Applications to Carbonatites. In: *Morphology and Phase Equilibria of Minerals. Proceedings of the 13th General Meeting of the International Mineralogical Association (September 19–25, 1982, Varna)*. Bulgarian Academy of Science, Sofia, Bulgaria, p. 313–322.

Fedorovsky V.S., Dobrzhinetskaya L.F., Molchanova T.V., Likhachev A.B., 1993. A New Type of Melange (Baikal, Olkhon Region). *Geotectonics* 4, 30–45 (in Russian) [Федоровский В.С., Добржинецкая Л.Ф., Молчанова Т.В., Лихачев А.Б. Новый тип меланжа (Байкал, Ольхонский регион) // Геотектоника. 1993. Т. 27. № 4. С. 30–45].

Fedorovsky V.S., Mazukabzov A.M., Sklyarov E.V., Gladkochub D.P., Donskaya T.V., Lavrenchuk A.V., Agatova A.R., Kotov A.B., 2012. *Aerospace Geological Map South-West Part of Chernorud and Tomota Zone of Olkhon Region (Lake Baikal)*. A1TIS Group, Moscow.

Fedorovsky V.S., Sklyarov E.V., 2010. The Olkhon Geodynamic Proving Ground (Lake Baikal): High-Resolution Satellite Data and Geological Maps of New Generation. *Geodynamics & Tectonophysics* 1 (4), 331–418 (in Russian) [Федоровский В.С., Склярлов Е.В. Ольхонский геодинамический полигон (Байкал): аэрокосмические данные высокого разрешения и геологические карты нового поколения // Геодинамика и тектонофизика. 2010. Т. 1. № 4. С. 331–418]. <https://doi.org/10.5800/GT-2010-1-4-0026>.

Fedorovsky V.S., Sklyarov E.V., Gladkochub D.P., Mazukabzov A.M., Donskaya T.V., Lavrenchuk A.V., Starikova A.E., Dobretsov N.L., Kotov A.B., Tevelev Ark.V., 2017. Aerospace Geological Map of the Olkhon Region (Baikal, Russia). Copymaster Center, Moscow.

Fedorovsky V.S., Sklyarov E.V., Gladkochub D.P., Mazukabzov A.M., Donskaya T.V., Lavrenchuk A.V., Starikova A.E., Dobretsov N.L., Kotov A.B., Tevelev Ark.V., 2020. Collision System of West Pribaikalie: Aerospace Geological Map of Olkhon Region (Baikal, Russia). *Geodynamics & Tectonophysics* 11 (3), 447–452 (in Russian) [Федоровский В.С., Склярлов Е.В., Гладкочук Д.П., Мазукабзов А.М., Донская Т.В., Лавренчук А.В., Старикова А.Е., Добрецов Н.Л., Котов А.Б., Тевелев Арк.В. Коллизионная система Западного Прибайкалья: Аэрокосмическая геологическая карта Ольхонского региона (Байкал, Россия) // Геодинамика и тектонофизика. 2020. Т. 11. № 3. С. 447–452]. <https://doi.org/10.5800/GT-2020-11-3-0485>.

Fedorovsky V.S., Sklyarov E.V., Izokh A.E., Kotov A.B., Lavrenchuk A.V., Mazukabzov A.M., 2010. Strike-Slip Tectonics and Subalkaline Mafic Magmatism in the Early Paleozoic Collisional System of the Western Baikal Region. *Russian Geology and Geophysics* 51 (5), 534–547. <https://doi.org/10.1016/j.rgg.2010.04.009>.

Fedorovsky V.S., Vladimirov A.G., Khain E.V., Kargopolov S.A., Gibsher A.S., Izokh A.E., 1995. Tectonics, Metamorphism, and Magmatism of Collision Zones in Early Paleozoic Orogenic Complexes of Central Asia. *Geotectonics* 3, 3–22 (in Russian) [Федоровский В.С., Владимиров А.Г., Хаин Е.В., Каргополов С.А., Гибшер А.С., Изох А.Э. Тектоника, метаморфизм и магматизм коллизионных зон каледонид Центральной Азии // Геотектоника. 1995. Т. 29. № 3. С. 3–22].

Gladkochub D.P., Donskaya T.V., Fedorovskii V.S., Mazukabzov A.M., Sklyarov E.V., Lavrenchuk A.V., Lepekhina E.N., 2014. Fragment of the Early Paleozoic (~500 Ma) Island Arc in the Structure of the Olkhon Terrane, Central Asian Fold Belt. *Doklady Earth Sciences* 457, 905–909. <https://doi.org/10.1134/S1028334X14080042>.

Lavrenchuk A.V., Sklyarov E.V., Izokh A.E., Kotov A.B., Sal'nikova E.B., Fedorovsky V.S., Mazukabzov A.M., 2017. Compositions of Gabbro Intrusions in the Krestovsky Zone (Western Baikal Region): A Record of Plume–Suprasubduction Mantle Interaction. *Russian Geology and Geophysics* 58 (10) 1139–1153. <https://doi.org/10.1016/j.rgg.2017.09.001>.

Lavrenchuk A.V., Sklyarov E.V., Izokh A.E., Kotov A.B., Vasyukova E.A., Fedorovskii V.S., Gladkochub D.P., Donskaya T.V., Mazukabzov A.M., 2019. Birkhin Volcanoplutonic Association, Ol'khon Region, Western Baikal Area: Petrological Criteria of Comagmatic Origin. *Petrology* 27, 291–306. <https://doi.org/10.1134/S0869591119030044>.

Lentz D.R., 1999. Carbonatite Genesis: A Reexamination of the Role of Intrusion-Related Pneumatolytic Skarn

Processes in Limestone Melting. *Geology* 27 (4), 335–338. [https://doi.org/10.1130/0091-7613\(1999\)027%3C0335:CGAROT%3E2.3.CO;2](https://doi.org/10.1130/0091-7613(1999)027%3C0335:CGAROT%3E2.3.CO;2).

Liu Y., Berner Z., Massonne H.-J., Zhong D., 2006. Carbonatite-Like Dykes from the Eastern Himalayan Syn-taxis: Geochemical, Isotopic, and Petrogenetic Evidence for Melting of Metasedimentary Carbonate Rocks within the Orogenic Crust. *Journal of Asian Earth Sciences* 26 (1), 105–120. <https://doi.org/10.1016/j.jseaes.2004.10.003>.

Patino Douce A.E., Harris N., 1998. Experimental Constraints on Himalayan Anatexis. *Journal of Petrology* 39 (4), 689–710. <https://doi.org/10.1093/петрол/39.4.689>.

Pavlovsky E.V., Eskin A.S., 1964. Archean Rocks in the Baikal Region: Composition and Structure. Nauka, Moscow, 128 p. (in Russian) [Павловский Е.В., Ескин А.С. Особенности состава и структуры архея Прибайкалья. М.: Наука, 1964. 128 с.].

Roberts D., Zwaan K.B., 2007. Marble Dykes Emanating from Marble Layers in an Amphibolite-Facies, Multiply-Deformed Carbonate Succession, Troms, Northern Norway. *Geological Magazine* 144 (5), 883–888. <https://doi.org/10.1017/S0016756807003810>.

Sklyarov E.V. (Ed.), 2005. Structural and Tectonic Correlation across the Central Asia Orogenic Collage: North-Eastern Segment. Guidebook and Abstract Volume of the Siberian Workshop IGCP480 (July 25 – August 6, 2005, Irkutsk – Ulan-Ude, Russia). IEC SB RAS, Irkutsk, 291 p.

Sklyarov E.V., Fedorovsky V.S., Kotov A.B., Lavrenchuk A.V., Mazukabzov A.M., Levitsky V.I., Sal'nikova E.B., Starikova A.E. et al., 2009. Carbonatites in Collisional Settings and Pseudo-Carbonatites of the Early Paleozoic Ol'khon Collisional System. *Russian Geology and Geophysics* 50 (12), 1091–1106. <https://doi.org/10.1016/j.rgg.2009.11.008>.

Sklyarov E.V., Fedorovsky V.S., Kotov A.B., Lavrenchuk A.V., Mazukabzov A.M., Starikova A.E., Yakovleva S.Z., Anisimova I.V., Fedoseenko A.M., 2013. Carbonate and Silicate-Carbonate Injection Complexes in Collision Systems: The West Baikal Region as an Example. *Geotectonics* 47 (3), 180–196. <https://doi.org/10.1134/S0016852113020064>.

Sklyarov E.V., Lavrenchuk A.V., Fedorovsky V.S., Pushkarrev E.V., Semenova D.V., Starikova A.E., 2020. Dismembered Ophiolite of the Olkhon Composite Terrane (Baikal, Russia): Petrology and Emplacement. *Minerals* 10 (4), 305. <https://doi.org/10.3390/min10040305>.

Sklyarov E.V., Lavrenchuk A.V., Mazukabzov A.M., 2021. Marble Mélange: Variations of Composition and Modes of Formation. *Geodynamics & Tectonophysics* 12 (4), 805–825 (in Russian) [Склярлов Е.В., Лавренчук А.В., Мазукабзов А.М. Мраморный меланж: вариации состава и механизмы образования // Геодинамика и тектонофизика. 2021. Т. 12. № 4. С. 805–825]. <https://doi.org/10.5800/GT-2021-12-4-0556>.

Vuorinen J.H., Skelton A.D.L., 2004. Origin of Silicate Minerals in Carbonatites from Alno Island, Sweden: Magmatic Crystallization or Wall Rock Assimilation. *Terra Nova* 16 (4), 210–215. <https://doi.org/10.1111/j.1365-3121.2004.00557.x>.

Wan Y., Liu D., Xu Z., Dong C., Wang Z., Zhou H., Yang Z., Liu Z., Wu J., 2008. Paleoproterozoic Crustally Derived Carbonate-Rich Magmatic Rocks from the Daqinshan Area, North China Craton: Geological, Petrographical, Geochronological and Geochemical (Hf, Nd, O and C) Evidence. *American*

Journal of Science 308 (3), 351–378. <https://doi.org/10.2475/03.2008.07>.

Wyllie P.J., Tuttle O.F., 1960. The System CaO-CO₂-H₂O and the Origin of Carbonatites. *Journal of Petrology* 1 (1), 1–46. <https://doi.org/10.1093/petrology/1.1.1>.

Yarmolyuk V.V., Kuz'min M.I., Vorontsov A.A., 2013. West Pacific-Type Convergent Boundaries and Their Role in the Formation of the Central Asian Fold Belt. *Russian Geology and Geophysics* 54 (12), 1427–1441. <https://doi.org/10.1016/j.rgg.2013.10.012>.

Table 1.1. Mineral chemistry of garnets from calc-silicate rocks

Component	Site 1								Site 3							
	1	2	3	4	5	6	7	8	1	2	3	4	5	6	7	8
SiO ₂	39.32	39.54	39.21	38.93	38.32	37.61	37.64	36.71	39.60	39.17	39.62	39.30	39.04	39.15	38.09	38.79
TiO ₂	bdl	bdl	bdl	bdl	0.32	1.48	0.33	2.14	bdl	bdl	bdl	bdl	bdl	bdl	0.95	0.33
Al ₂ O ₃	22.09	21.62	19.72	19.42	17.10	15.89	15.21	12.51	21.41	20.97	19.88	19.16	18.37	18.04	16.51	15.02
FeO _{tot}	0.11	1.27	3.09	4.49	6.46	7.78	9.31	11.63	1.67	2.15	3.94	4.86	5.61	6.34	7.90	9.53
MnO	bdl	bdl	bdl	0.39	0.44	0.41	0.37	0.36	bdl	bdl	bdl	bdl	bdl	bdl	bdl	bdl
MgO	bdl	bdl	bdl	bdl	bdl	0.38	bdl	0.50	bdl	bdl	bdl	bdl	bdl	bdl	bdl	bdl
CaO	36.67	36.84	36.45	35.95	35.58	35.20	34.90	34.61	36.82	36.26	36.81	36.51	36.30	36.25	36.04	36.03
Total	98.19	99.46	98.47	98.78	98.22	98.17	97.76	98.46	99.50	98.55	100.25	99.83	99.32	99.78	99.49	99.70
	O=12															
Si	3.003	2.996	3.013	2.982	2.987	2.933	2.972	2.910	2.997	2.997	2.996	2.992	2.995	2.995	2.944	3.003
Ti	0.000	0.000	0.000	0.000	0.019	0.087	0.020	0.128	0.000	0.000	0.000	0.000	0.000	0.000	0.055	0.019
Al	1.989	1.932	1.787	1.754	1.572	1.461	1.416	1.169	1.911	1.892	1.772	1.720	1.661	1.627	1.505	1.371
Fe ³⁺	0.005	0.075	0.187	0.282	0.416	0.500	0.601	0.756	0.095	0.113	0.236	0.296	0.349	0.382	0.496	0.584
Fe ²⁺	0.002	0.005	0.012	0.006	0.005	0.007	0.014	0.015	0.011	0.024	0.013	0.014	0.011	0.024	0.014	0.033
Mn	0.000	0.000	0.000	0.025	0.029	0.027	0.025	0.024	0.000	0.000	0.000	0.000	0.000	0.000	0.000	0.000
Mg	0.000	0.000	0.000	0.000	0.000	0.044	0.000	0.059	0.000	0.000	0.000	0.000	0.000	0.000	0.000	0.000
Ca	3.001	2.991	3.001	2.951	2.972	2.941	2.953	2.940	2.986	2.973	2.983	2.979	2.984	2.972	2.985	2.989
Total	8.000	8.000	8.000	8.000	8.000	8.000	8.000	8.000	8.000	8.000	8.000	8.000	8.000	8.000	8.000	8.000
X _{Andr}	0.00	0.04	0.09	0.14	0.21	0.26	0.30	0.39	0.05	0.06	0.12	0.15	0.17	0.19	0.25	0.30
X _{Grs}	1.00	0.96	0.91	0.86	0.79	0.74	0.70	0.61	0.95	0.94	0.88	0.85	0.83	0.81	0.75	0.70

Note. bdl – below detection limit; content of Cr₂O₃, Na₂O, K₂O below detection limit.

Table 1.2. Mineral chemistry of pyroxenes from calc-silicate rocks

Component	Site 1									Site 3						
	1	2	3	4	5	6	7	8	9	1	2	3	4	5	6	7
SiO ₂	52.91	53.77	53.51	52.88	52.76	52.73	51.28	52.37	50.83	53.19	52.02	52.01	51.46	50.89	50.27	49.61
TiO ₂	bdl	bdl	bdl	bdl	bdl	bdl	bdl	bdl	bdl	bdl	bdl	bdl	bdl	bdl	bdl	bdl
Al ₂ O ₃	0.32	0.00	0.38	0.96	0.30	0.38	0.53	1.19	1.23	0.55	0.57	0.66	0.00	0.00	0.00	0.40
Cr ₂ O ₃	bdl	bdl	bdl	bdl	bdl	bdl	bdl	bdl	bdl	bdl	bdl	bdl	bdl	bdl	bdl	bdl
FeO _{tot}	4.67	5.63	6.23	7.55	9.24	10.01	11.49	13.80	21.60	8.88	10.55	13.68	15.49	17.41	20.79	23.44
MnO	0.31	0.40	0.39	bdl	0.41	0.46	0.61	bdl	bdl	bdl	bdl	bdl	bdl	bdl	bdl	bdl
MgO	14.85	14.00	14.23	12.77	12.31	11.44	10.75	9.35	4.74	12.80	11.60	9.67	8.51	7.13	5.14	3.65
CaO	25.03	25.44	24.99	24.53	24.60	25.23	23.81	22.64	21.72	25.03	24.18	24.52	24.11	24.03	23.70	23.02
Na ₂ O	bdl	0.25	bdl	0.39	bdl	bdl	bdl	0.89	0.66	bdl	bdl	bdl	bdl	bdl	bdl	bdl
K ₂ O	bdl	bdl	bdl	bdl	bdl	bdl	bdl	bdl	bdl	bdl	bdl	bdl	bdl	bdl	bdl	bdl
Total	98.09	99.49	99.73	99.08	99.62	100.25	98.47	100.24	100.78	100.45	98.92	100.54	99.57	99.46	99.90	100.12
O=6																
Si	1.989	2.002	1.991	1.988	1.993	1.989	1.981	1.991	1.994	1.985	1.987	1.983	2.000	1.999	1.997	1.989
Ti	0.000	0.000	0.000	0.000	0.000	0.000	0.000	0.000	0.000	0.000	0.000	0.000	0.000	0.000	0.000	0.000
Al	0.014	0.000	0.017	0.043	0.013	0.017	0.024	0.053	0.057	0.024	0.026	0.030	0.000	0.000	0.000	0.019
Cr	0.000	0.000	0.000	0.000	0.000	0.000	0.000	0.000	0.000	0.000	0.000	0.000	0.000	0.000	0.000	0.000
Fe ³⁺	0.008	0.014	0.001	0.010	0.001	0.004	0.015	0.031	0.005	0.005	0.000	0.004	0.000	0.002	0.007	0.004
Fe ²⁺	0.139	0.162	0.193	0.228	0.291	0.312	0.356	0.408	0.704	0.272	0.337	0.432	0.503	0.570	0.684	0.782
Mn	0.010	0.013	0.012	0.000	0.013	0.015	0.020	0.000	0.000	0.000	0.000	0.000	0.000	0.000	0.000	0.000
Mg	0.832	0.777	0.789	0.715	0.693	0.643	0.619	0.530	0.277	0.712	0.660	0.549	0.493	0.417	0.304	0.218
Ca	1.008	1.015	0.997	0.988	0.996	1.020	0.985	0.922	0.913	1.001	0.990	1.002	1.004	1.011	1.009	0.989
Na	0.000	0.018	0.000	0.028	0.000	0.000	0.000	0.066	0.050	0.000	0.000	0.000	0.000	0.000	0.000	0.000
K	0.000	0.000	0.000	0.000	0.000	0.000	0.000	0.000	0.000	0.000	0.000	0.000	0.000	0.000	0.000	0.000
Total	4.000	4.000	4.000	4.000	4.000	4.000	4.000	4.000	4.000	4.000	4.000	4.000	4.000	4.000	4.000	4.000
X _{Mg}	0.85	0.82	0.79	0.76	0.69	0.66	0.62	0.57	0.28	0.72	0.66	0.56	0.49	0.42	0.31	0.22

Note. bdl – below detection limit; X_{Mg}=Mg/(Mg+Mn+Fe²⁺).

Table 1.3. Mineral chemistry of allanite and zoizite from calc-silicate rocks

Component	Site 1					Site 3			
	1	2	3	4	5	1	2	3	4
SiO ₂	34.17	33.82	33.74	33.78	32.07	39.24	38.47	38.88	38.70
Al ₂ O ₃	21.52	21.26	21.80	20.48	18.27	31.91	30.55	29.88	27.57
FeO	10.99	9.20	8.17	9.49	9.12	1.04	3.54	4.73	6.32
MgO	bdl	bdl	bdl	0.53	bdl	bdl	bdl	bdl	bdl
CaO	17.25	16.38	15.49	14.45	19.52	24.42	24.05	24.12	24.01
Ce ₂ O ₃	7.20	10.88	9.50	10.08	11.24	bdl	bdl	bdl	bdl
La ₂ O ₃	5.31	6.53	5.02	8.12	5.42	bdl	bdl	bdl	bdl
Pr ₂ O ₃	0.00	0.00	1.59	0.00	1.47	bdl	bdl	bdl	bdl
Nd ₂ O ₃	1.17	1.53	3.37	1.89	3.70	bdl	bdl	bdl	bdl
Total	97.61	99.60	98.68	98.83	100.82	96.61	96.61	97.61	96.60
REE	13.68	18.94	19.48	20.09	21.83	0.00	0.00	0.00	0.00

O=25									
Si	6.033	6.002	6.019	6.074	5.855	6.043	5.974	5.995	6.066
Al	4.479	4.446	4.585	4.341	3.931	5.794	5.593	5.431	5.095
Fe ³⁺	1.623	1.365	1.219	1.428	1.393	0.129	0.441	0.585	0.795
Mg	0.000	0.000	0.000	0.142	0.000	0.000	0.000	0.000	0.000
Ca	3.264	3.115	2.961	2.785	3.818	4.030	4.002	3.985	4.033
Ce	0.466	0.707	0.620	0.664	0.752	0.000	0.000	0.000	0.000
La	0.346	0.428	0.330	0.538	0.365	0.000	0.000	0.000	0.000
Pr	0.000	0.000	0.103	0.000	0.098	0.000	0.000	0.000	0.000
Nd	0.074	0.097	0.215	0.121	0.241	0.000	0.000	0.000	0.000
Total	16.284	16.159	16.053	16.093	16.452	15.996	16.009	15.997	15.989

Note. bdl – below detection limit; content of TiO₂, Cr₂O₃, FeO, MnO, Na₂O, K₂O below detection limit.

Table 1.4. Mineral chemistry of K-feldspar from calc-silicate rocks

Component	Site 1					Site 3	
	1	2	3	4	5	1	2
SiO ₂	64.24	64.36	64.46	64.06	64.28	64.52	64.11
Al ₂ O ₃	18.69	18.78	17.44	18.28	18.21	18.21	18.82
Na ₂ O	0.33	bdl	bdl	0.37	0.34	0.55	bdl
K ₂ O	15.80	16.48	16.97	16.59	15.32	16.13	16.97
BaO	3.27	1.80	0.00	0.76	4.30	bdl	bdl
Total	99.06	99.62	98.87	99.30	98.15	99.41	99.90

O=8							
Si	2.964	2.972	3.023	2.984	2.977	3.000	2.976
Al	1.017	1.022	0.964	1.004	0.994	0.998	1.030
Na	0.030	0.000	0.000	0.033	0.031	0.050	0.000
K	0.930	0.971	1.015	0.986	0.905	0.957	1.005
Ba	0.066	0.036	0.000	0.015	0.087	0.000	0.000
Total	5.007	5.002	5.003	5.023	4.994	5.004	5.011

Note. bdl – below detection limit; content of TiO₂, Cr₂O₃, FeO, MnO, MgO below detection limit.

Table 1.5. Chemistry of marble and carbonate-silicate dikes

Sample	Site 1		Site 2			Site 3		Site 4		
	09A160A centre	09A160B rim	SE1152A centre	SE1152B rim	SE742A	SE1504C	SE1507A	SE724A	SE725A	SE725B
SiO ₂	8.83	20.17	4.83	6.75	2.26	1.09	4.45	4.60	0.00	1.10
TiO ₂	0.12	0.26	0.00	0.49	0.03	0.00	0.05	0.03	0.03	0.03
Al ₂ O ₃	1.82	4.16	0.22	1.71	0.25	0.00	0.70	0.30	0.15	0.00
Fe ₂ O ₃	0.27	0.72	0.14	0.51	0.18	0.00	0.66	0.20	0.20	0.20
FeO	0.81	1.23	0.62	1.73	0.00	0.00	0.00	0.00	0.00	0.00
MnO	0.12	0.13	0.04	0.06	0.00	0.01	0.00	0.07	0.00	0.00
MgO	2.78	5.01	0.26	1.04	0.00	0.55	0.64	2.20	20.39	22.58
CaO	48.26	40.72	52.49	49.25	54.55	54.78	52.84	52.12	33.45	31.99
Na ₂ O	0.23	0.53	0.05	0.46	0.03	0.00	0.08	0.00	0.00	0.00
K ₂ O	0.33	0.32	0.04	0.01	0.02	0.00	0.11	0.02	0.01	0.00
P ₂ O ₅	0.04	0.09	0.10	0.08	0.03	0.03	0.05	0.04	0.00	0.00
H ₂ O	0.10	0.13	0.06	0.06	0.06	0.03	0.00	0.00	0.00	0.00
CO ₂	35.80	25.78	41.18	36.85	42.37	42.82	39.79	40.34	45.49	40.70
LOI	0.40	0.69	0.00	1.17	0.00	0.57	0.52	0.00	0.00	3.32
Total	100.01	100.04	100.19	100.28	99.78	100.34	100.13	99.92	99.72	100.00
Sr	510	400	1400	930	2900	1500	2300	540	37	58
Ba	310	380	n.d.	n.d.	n.d.	n.d.	n.d.	n.d.	n.d.	n.d.

Note. n.d. – not determined.